A comparative study of online State-of-Health estimation algorithms for Lithium-ion batteries

Dadhekar, Kshitij

Award date:
2020

A comparative study of online State-of-Health estimation algorithms for Lithium-ion batteries

Kshitij Dadhekar
MSc. Thesis
Technische Universiteit Eindhoven

***Abstract*—Estimation of the internal states of Lithium-ion batteries (LiB) plays a crucial role in modern-day Battery Management Systems (BMSs). For example, besides the State-of-Charge estimation that reflects how much charge is currently stored, the State-of-Health estimation is used to quantify the extent of capacity fade and power fade of a LiB. In this paper, a comparative study of several SoH algorithms that can be used in a BMS is done. Kalman filter (KF) and Least-squares (LS) variants are implemented and tested on simulated data-sets. Validation of various algorithms on the same test-data allows comparison on performance based on estimation accuracy. Besides this, differences in computational complexity and implementation details in an embedded system are addressed.**

***Index Terms*—State-of-Health estimation, Battery Management Systems, Algorithms, Embedded Systems.**

I. Introduction

Lithium-ion Batteries (LiBs) are manufactured in various form factors, and every use case needs a tailor-made solution. LiB safety and management systems need to be designed meticulously. A Lithium-ion (Li-ion) cell is the fundamental unit of a LiB pack. These cells are connected in a particular series and parallel combination to achieve the required voltage and capacity. It is important to monitor every cell in the pack to get an accurate estimate of the pack's status. Therefore, much research is carried out on the cell level and then generalized to the pack level. As the relation between the capacity in the cell and voltage is described by a non-linear curve, one of the ways to model the cell is as a non-linear system. Li-ion cell measurements are used to characterize the cell's behavior. Based on this, a non-linear model is constructed to estimate the State-of-Charge (SoC), State-of-Health (SoH), State-of-Function (SoF), etc. A combination of the cell's non-linear model with real-time measurements can be used in an estimation algorithm to get an accurate estimate.

Degradation occurs when the cell is cycled and/or stored for a certain period of time. As a result, the cell loses its maximum capacity and its impedance rises due to several electrochemical reactions. To estimate these, SoH estimation algorithms are used. The SoF is generally defined as the ability of the battery to deliver a certain amount of power given the battery's current SoC and SoH. Therefore, if the SoH estimation is not accurate this can lead to a faulty SoF estimation. It is therefore crucial to estimate SoH using a robust estimation algorithm.

There has been extensive research in the field of modeling and state estimations of LiBs. A lot of this work is spread across various specializations and applications of LiBs. As the goal of this research is to focus on State-of-Health estimation algorithms for use in vehicles that range from Light Electric Vehicles (LEVs) to electric trucks and buses, it was necessary to select algorithms and paradigms that are efficient enough to be implemented on an embedded micro-controller with a processing speed of a few hundred MHz. Krewer et al. [1] presented an extensive overview of all the dynamic modeling techniques used to model a Li-ion cell and the possible ways to use these models with algorithms for SoC and SoH estimation. Farmann et a parl. [2] presented a critical review of capacity estimation techniques for SoH estimation. The Kalman Filter (KF) and its extended variants are widely used for these state estimations. Plett [3] presented the use of an Extended Kalman Filter (EKF) for estimating the capacity and the impedance of a Li-ion cell. Fang et al. [4] present a Dual EKF (DEKF) for estimating SoH based on the cell impedance. Plett [5] presented another methodology with a Least-Squares (LS) algorithm to estimate the capacity. Liu et al. [6] presented the use of an Unscented-Particle-Filter algorithm for estimating capacity for SoH estimation. Harting et al. [7] presented a novel way to estimate SoH with non-linear frequency response analysis and a Support-Vector-Machine algorithm. Berecibar et al. [8] showed the use of differential voltage curves of LiBs for SoH estimation algorithms.

The primary focus of this study is to implement and compare algorithms for SoH estimation. This is done in order to gain insights about the algorithm's behavior in various (dis)charge and storage conditions. Secondly, these SoH estimation algorithms will be compared based on their computational and implementation complexity on an embedded micro-controller. The paper is structured as follows. Section II talks about degradation in LiBs and problems with existing solutions. Section III talks about all the parameters that affect the State-of-Health of a LiB. Section IV talks about various algorithms used in practice for SoH estimation along with degradation models. Section V presents a comparison of a selected few SoH algorithms. Section VI elaborates on how these SoH estimation algorithms can be implemented on an embedded system with limited processing power and memory. Lastly, section VII presents the conclusions.

II. Trends in LiB degradation and SoH estimation

Analyzing Li-ion cell aging data and modeling its aging behavior has picked up pace over the past decade. This has

given impetus to gain insights about the factors affecting the degradation in LiBs. It is rather important to factor all the possible causes of degradation in order to have exact knowledge about the battery pack's health. The following subsections elaborate on degradation in LiBs and the problems with the present solutions.

A. Degradation in LiBs

Degradation in LiBs has been studied thoroughly and some relevant literature can be found. Birkl et al. [9] presented causes for degradation in LiBs along with diagnostic methods. Fig. 1 presents an overview of the possible factors that influence LiB degradation. There are four aspects affecting the degradation, namely cycle aging, calendar aging, loss of cell materials and environmental factors.

On a component level, the Li-ion cell experiences degradation by the loss of active material at the anode and at the cathode. This loss of active material is one of the reasons resulting in the loss of Lithium inventory (number of Li-ions). Based on the usage/storage conditions, these three entities are affected and they ultimately result in either capacity fade or power fade.

Cycling a Li-ion cell to a certain DoD around a particular average SoC or voltage and at a certain C-rate accounts for cycle aging. From [10], it was concluded that cycling at an average SoC of 10% or 90% results in higher degradation whereas cycling at an average SoC of 50% results in a comparatively lower degradation in terms of both capacity fade and power fade. Cycling to a higher DoD results in higher degradation.

Storing a Li-ion cell at a particular SoC/voltage and temperature is identified as Calendar aging. From [10], it was concluded that storing at higher SoC/voltage (80% - 100%) at a higher temperature (45°C - 50°C) results in higher degradation. The dominant calendar aging mechanism is the formation of Solid Electrolyte Interphase between the electrolyte and the active (electrode) materials. This results in an irreversible loss of available Li-ions that are used for cycling ultimately resulting in capacity fade.

Lastly, the environmental factors and usage of the LiB affects the degradation rate of the Li-ion cells based on factors like mechanical stress. Often, battery packs are required to be heated/cooled given the operating environmental conditions and the required SoF. This is needed as the operational and/or ambient temperature is one of the major factors affecting the SoH of a LiB pack. It can be said that the degradation caused by cycle and calendar aging is affected by these environmental factors as well. It is therefore crucial to account for calendar and cycle aging for a better SoH estimation.

B. Problems with present solutions

Typically, the capacity and/or impedance estimations of a the Li-ion cell is used to estimate the SoH. If the SoH estimation is not accurate or is erratic, the amount of power and energy that can be drawn from the system can also become erroneous. This is because several advanced BMSs limits the amount of power and energy consumption based on this SoH estimation. One such example of an erroneous SoH estimation is presented in Fig. 2. Here, the SoH is estimated by Texas Instrument's [11] Impedance Track BQ series chip. These are Integrated Circuits (ICs) that can be used on a pack-level. These ICs provide a combined solution for estimating SoC and SoH based on the voltage drop across a sense resistor. The measurement data shown in Fig. 2 is obtained from a 48 V 1.5 kWh pack manufactured by Cleantron Cleantech Batteries. The pack was cycled with 15 A discharge pulses (60 seconds) and 10 A charge pulses (30 seconds) at room temperature. It can be observed that for a test duration of 3000 seconds, the SoH fluctuates with a maximum difference of 5%. In a lot of applications, SoH is an integral input for the SoF estimation. This fluctuation of 5% will result in a erroneous SoF estimation as well.

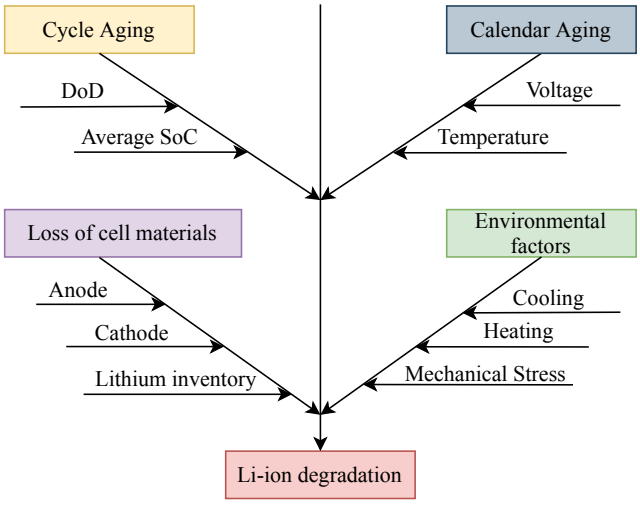

Fig. 1. Factors affecting Li-ion cell degradation (derived from [7] and [9]).

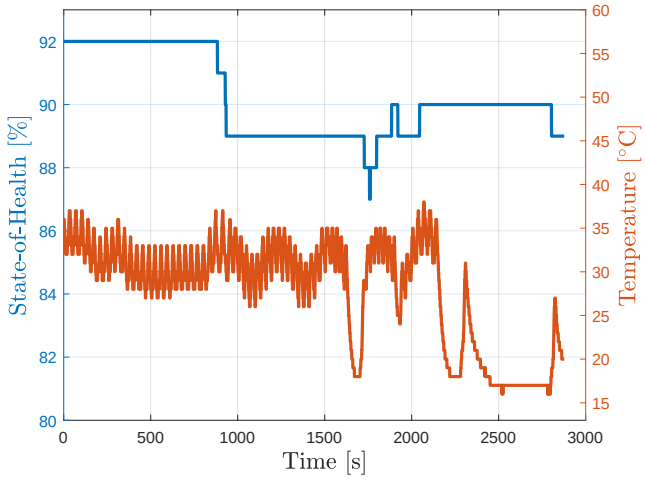

Fig. 2. Fluctuating and erratic behavior of SoH estimation using Texas Instrument's impedance based fuel gauge solution.

III. State-of-Health estimation methodology of Lithium-ion batteries

State estimations like SoH are required as the true states of a Li-ion cell like number of Li-ions or the loss of active electrode material cannot be measured. Therefore, when it comes to a Li-ion cell and a BMS, there are real/true values, measured values and estimated values. Based on these, several SoH estimation methodologies can be achieved. The true values are based on the chemical composition of the Li-ion cell. For example, the number of Lithium ions in the cell which build up the charge and the potential difference across the cell's terminals. As the internal true values are not accessible across the cell terminals, measuring the number of Li-ions is not possible. Therefore, Analog Front-End (AFE) devices are used to measure the voltage, current and temperature from the cell's terminals/surface. The AFE functionality is a subset of a BMS that gives us the measured values. The SoC, SoH and SoF are derived and estimated values based on the AFE's measured values. Fig. 3 presents the order and layout of these real, measured and estimated values.

The measured voltage and current values are firstly used as input for SoC estimation. The SoC estimation (0%-100%) gives an estimate of the charge left in the cell as a ratio to the maximum available charge under defined conditions. This SoC estimation can be used as input for estimating the SoH and SoF. The SoF estimation is the readiness of the LiB to deliver a certain amount of power given the present state (SoC and SoH) and the ambient temperature. The SoH estimation is also used an input for EoL prediction and EoL extension. The SoH estimation tells us about the present age of the cell while EoL prediction tells us about the Remaining Useful Life in terms of charge throughput of the cell.

There are numerous ways to estimate the State of Health of a Li-ion cell. Fig. 4 presents a paradigm for SoH estimation. Firstly, the cell's voltage, current and the temperature need

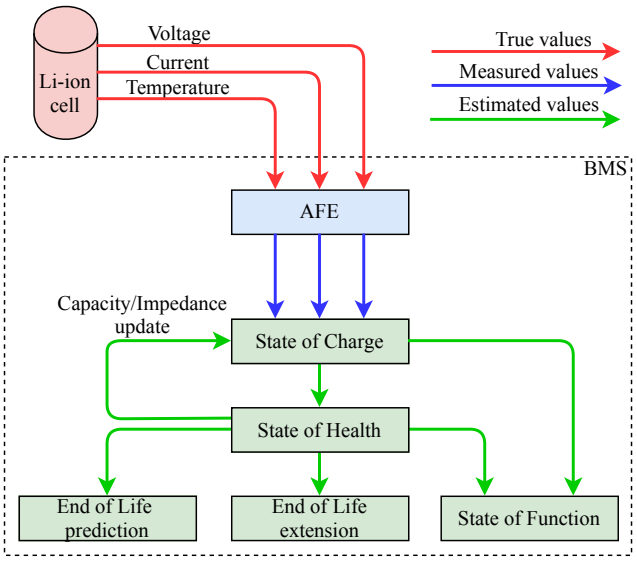

Fig. 3. True, measured and estimated values of a Li-ion cell.

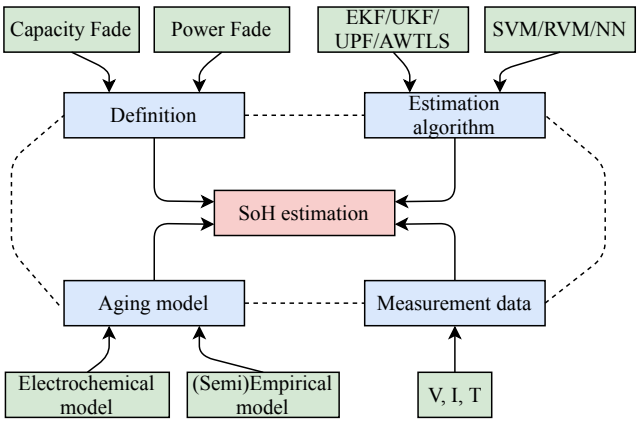

Fig. 4. An overview of the State-of-Health estimation paradigm with interlinked modules.

to be measured at a certain frequency for the SoH estimation. This is obtained by the BMS from its AFE IC. Nowadays, [12] AFEs provide functionality for measuring voltage, current and temperature synchronously. This is useful for LiBs where there are large number of cells in series. SLIDE [13] (**S**imulator for **Li**thium-ion **De**gradation), is a Li-ion cell simulation software that can be used to generate cycling and aging data of a Li-ion cell. SLIDE uses electrochemical models of a Li-ion cell to simulate aging behavior of a cell. For this study, simulated cell aging data generated from SLIDE will be used as voltage, current and temperature measurements.

Secondly, the SoH needs to be defined precisely. On one hand, SoH can be defined based on capacity fade as expressed as:

$$SoH = \frac{Q_{\text{now}}}{Q_{\text{BoL}}} \times 100\% \tag{1}$$

where, Q_{now} is the cell's capacity at any given time instant during the cell's usage and Q_{BoL} is the cell's capacity [Ah] during the beginning of its life (BoL). There are several checkup procedures of obtaining Q_{now}. These differ from application to application. As the cell impedance also rises, the capacity obtained from these check-ups also factors in the power fade. If the capacity drops to 80% of its pristine state and the SoH is defined as per (1) then a SoH of 80% is considered as End-of-Life (EoL) Secondly, SoH can be defined based on the cell's impedance.

$$SoH = \frac{R_{\text{EoL}} - R_{\text{now}}}{R_{\text{EoL}} - R_{\text{BoL}}} \times 100\% \tag{2}$$

Where, R_{BoL} is the ohmic resistance at the BoL, R_{EoL} is the ohmic resistance of the cell at the EoL and R_{now} is the present ohmic resistance of the cell. It needs to be noted that according to (2), when $R_{\text{now}} = R_{\text{EoL}}$ the SoH = 0%. In this study, SoH defined as per (1) will be used by the SoH estimation algorithms.

Thirdly, an aging model that captures the cell's aging behavior at various cycling C rates, DoD, storage voltage, etc. can be used to get a better idea of the degradation pattern. There are various aging models presented in literature. Electrochemical

models provide better insights about cell degradation and aging but at the cost of computational complexity. On the other hand (semi)empirical models [13] give reasonable accuracy and are rather straight forward to characterize and implement on a BMS. One such example of a (semi)empirical model is presented by Schmalstieg et al. [10]. This model will be further described in section IV. Lastly, an estimation algorithm which takes into account all the three aforementioned modules needs to be selected in order to get a SoH estimation.

IV. Algortihms for SoH estimation

As the cell's voltage, current and temperature can be sampled at a rather high frequency, various mapping features/characteristics of the Li-ion cell can be constructed based on this measurement data. These mapping features are used as an input for the SoH estimation algorithm. Fig. 5 presents an inter-linked overview of these mapping features with SoH algorithms. Here, degradation models are considered as a part of the algorithms section. The gray links depict all the combinations found in literature and the black links depict the choices made for this study. There is no mapping feature constructed with temperature, instead it is directly used an input (red dot) for the KF variants algorithm. DV [8] and IC curves [14] can be used for an application where the cell is (dis)charged at a constant current. However, it is rather important to choose a mapping feature that captures the dynamic behavior of the cell based on varying current values like a drive cycle profile. Therefore, for this study, SoC and coulomb-counting will be used as a mapping features and as an input to the SoH algorithm. The varying current of a given drive cycle profile is already factored by both the SoC and coulomb-counting. It is therefore important to have an accurate and robust SoC estimation method. Beelen [15] presented a Joint Extended Kalman Filter with a cross-correlating forgetting factor (JEKFCF) that jointly estimates the SoC with its model parameters (first-order ECM model). The JEKFCF uses a cross-correlated noise and forgetting for the process and measurement noise co-variances that provides more robust estimation. The forgetting factor is the only tuning parameter and it allows for easier tuning. For the algorithms compared and tested in this study, coulomb-counting and SoC (estimated with JEKFCF) will be used as an input.

For an online real-time SoH estimation, the algorithms shown in Fig. 5 need to be implemented on an embedded micro-controller. Therefore, the computational complexity and memory footprint need to be taken into account before making a choice. The Least-Squares (LS) algorithms [5] and its variants are used to fit measurement data to a (non)linear function. Depending on the usage conditions, the cell's capacity degrades in a non-linear manner. Therefore the LS optimization needs to be performed iteratively. LS variants (with a recursive approach) largely include simple arithmetic operations like addition, multiplication, subtraction, and division. Therefore, a recursive LS solution with a low memory footprint is preferred. Secondly, the Kalman Filter (KF) and its non-linear extended variants are widely used in the field of state estimations in BMS. KFs provide a recursive Bayesian estimation approach for predicting and estimating an unknown state based on a

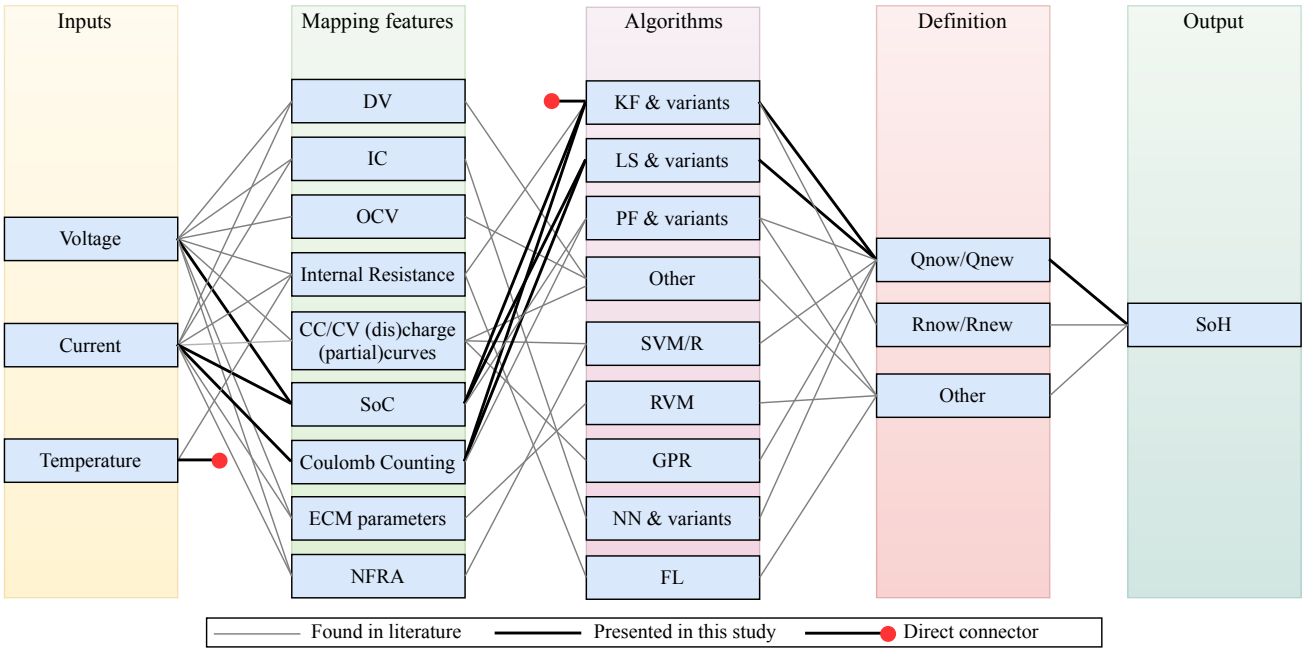

CC - Constant Current, CV - Constant Voltage, DV - Differential Voltage, ECM - Equivalent Circuit Model, FL - Fuzzy Logic, GPR - Gaussian Process Regression, IC - Incremental Capacity, KF - Kalman Filter, LS - Least Squares, NFRA - Non-linear Frequency Response Analysis, NN - Neural Network, OCV - Open Circuit Voltage, PF - Particle Filter, RVM - Relevance Vector Machine, SVM/R - Support Vector Machine/Regression

Fig. 5. Mapping features and algorithms for SoH estimation.

model of the system and real-time measurements. An Extended Kalman Filter (EKF) also has low computational complexity and can be easily implemented with C code on an embedded micro-controller [12]. Further, Sigma-Point KFs (SPKF) [16] can be used to improve the accuracy of the KF estimate. The SPKF variant provides more tuning parameters for Gaussian and non-Gaussian probability distribution functions (PDFs). An Unscented-Particle-Filter (UPF) [6] can also be used to estimate the capacity as well. The UPF is a combination of an SPKF and a bootstrapped Particle Filter [17]. This combination can provide a better estimate of the capacity as compared to the KF variants but the implementation is more complex. Therefore, the implementation of UPF is not considered for this study. Algorithms like the Support Vector Machine (SVM) [7] and Relevance Vector Machine (RVM) [18] are Machine Learning (ML) [19] variants used for supervised learning that offer classification and regression solutions. These algorithms need a large number of data sets for learning and training. The complexity of the Neural Network (NN) algorithms depends on a lot of factors such as the number of hidden layers. The computational complexity and the memory footprint of the inference part of these algorithms also need to be taken into account given the limitations of an embedded micro-controller. The NN can be pruned to reduce the computational complexity of the inference. As the goal of this study is to compare these algorithms based on their accuracy and computational complexity and not to optimize the NN variants for an embedded micro-controller, the ML and NN variants are not considered for the remainder of this study. Therefore, in the following subsections, an LS variant with three KF variants will be presented and evaluated.

A. Approximate Weighted Total Least Squares (AWTLS)

The LS regression approach can be used to fit and get an estimated capacity for a given set of SoC estimations and coulomb-counting measurements. The relation between SoC and coulomb-counting is given by:

$$z\left(t_2\right) = z\left(t_1\right) + \frac{1}{Q}\int_{t_1}^{t_2} \frac{\eta i(\tau)}{3600} d\tau, \tag{3}$$

where $z(t_1)$ is the estimated SoC at time t_1, $z(t_2)$ is the estimated SoC at time t_2, Q is capacity of the cell in Ampère-hours (Ah), η is the unitless coulombic efficiency of the cell (which changes w.r.t the sign of the current and age of the cell), $i(\tau)$ is the cell current (positive for charging) at time τ and t is time in seconds. The factor of 3600 is used to convert the Ampère-seconds to Ampère-hours. (3) can be re-arranged as:

$$\underbrace{\int_{t_1}^{t_2} \frac{\eta i(\tau)}{3600} d\tau}_{y} = Q(\underbrace{z\left(t_2\right) - z\left(t_1\right)}_{x}) \tag{4}$$

which is of the form $y = Qx$. Therefore, the coulomb-counting measurements (y) and difference between two SoC estimations (x) are of the form $\{x_i, y_i\} \mid i \in \{1, \ldots, N\}$ where N is the total number of input measurement/estimation pairs. The Ordinary Least-Squares (OLS) [5] methodology can be used to fit the coulomb-counting measurements (y-direction) against the SoC estimations (x-direction). It assumes that there is no SoC estimation error (x-direction) and uses only the uncertainty in the coulomb-counting measurements (y-direction). The Total Least-Squares (TLS) [5] approach on the other hand factors in both the errors in x and y direction. As the OLS approach does not take into account the uncertainties in the x-direction (caused by SoC estimations), it is not considered for the implementation. The TLS approaches can be generalized in such a way that the least-square minimization takes into account the sum of weighted squared errors. Here, the weight takes into account the uncertainty of coulomb-counting measurements as well as that of the SoC estimations. A merit function is constructed to measure the extent of agreement between the measurement/estimation data and the fitted model and it is given by

$$\chi^2_{\mathrm{WTLS}} = \sum_{i=1}^{N} \frac{\left(x_i - X_i\right)^2}{\sigma^2_{x_i}} + \frac{\left(y_i - Y_i\right)^2}{\sigma^2_{y_i}} \tag{5}$$

where σ_x is the variance of the SoC estimates and σ_y is the variance of coulomb-counting measurements. In (5), (X_i, Y_i) are points on the line $Y = \hat{Q}X$ corresponding to the measurement pair (x_i, y_i) as shown in Fig. 6 and $\hat{Q}$ is the estimated capacity. The WTLS approach assumes that the variances σ_x and σ_y are proportional to each other. In a practical EV scenario, the σ_x^2 and σ_y^2 are arbitrary and the WTLS approach does not allow to factor this arbitrary behavior. As an improvement in terms of factoring the arbitrary variances and accuracy, Plett [5] presented the Approximate Weighted Total Least Squares (AWTLS) algorithm for Li-ion capacity estimation. The AWTLS provides an approximated solution where the σ_x^2 and σ_y^2 can be non-proportional or unrelated to each other. However, it needs to be noted that as SoC estimators use

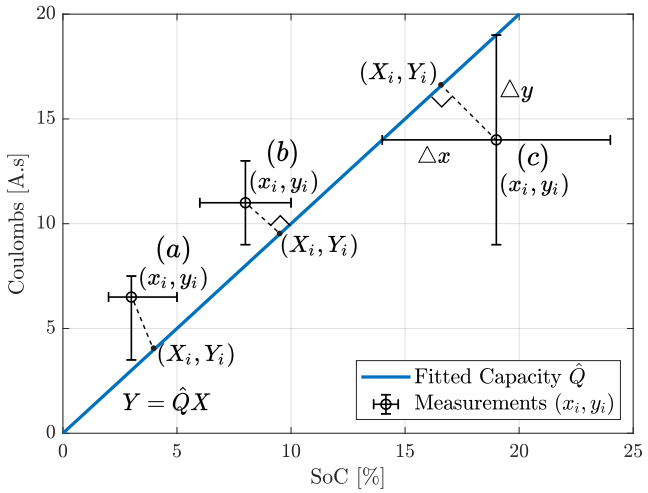

Fig. 6. A geometrical overview of the relationship between coulomb-counting measurements (y_i) and SoC estimations (x_i). Points (a) and (b) denote the mapping made by the WTLS with unequal and equal confidence on (x_i, y_i) respectively. Point (c) denotes definitions for derivation of AWTLS algorithm.

both coulomb-counting and the electromotive force (EMF), σ_x^2 and σ_y^2 may not be always unrelated to each other. Fig. 6 presents the geometry of the WTLS approach with the AWTLS derivation. Point (a) shows the WTLS relationship between the measurement/estimation pair (x_i, y_i) and its optimized map as per $Y = \hat{Q}X$ where $\hat{Q}$ is the estimated capacity. Here, the error bars on the data points show the uncertainty of SoC estimates in the x-direction and that of coulomb-counting measurement in the y-direction. For point (a), the distance of both these uncertainties is not necessarily equal. For a scenario where JEKFCF is used for SoC estimation, the variance/uncertainty of the x_i is exactly known, this can be used to calculate the near-exact difference between the measured value (x_i, y_i) and the fitted value (X_i, Y_i). For point (b), the two uncertainties are equal. The distance between x_i to X_i and y_i to Y_i is equal. The line joining these points is perpendicular. Therefore, if σ_x^2 and σ_y^2 are not equal then either the x-axis or y-axis can be scaled to get the new transformed points with equal variances for a better estimate. Furthermore, point (c) is used to enforce the fact that the line joining (x_i, y_i) and (X_i, Y_i) is perpendicular. This enables us to solve every new measurement point recursively to obtain $\hat{Q}$. The AWTLS cost function is illustrated as

$$\chi^2_{\text{AWTLS}} = \sum_{i=1}^{N} \gamma \frac{\left(y_i - \hat{Q}x_i\right)^2}{\left(1+\hat{Q}^2\right)^2} \left(\frac{\hat{Q}^2}{\sigma_{x_i}^2} + \frac{1}{\sigma_{y_i}^2}\right) \tag{6}$$

Here, the distances between (x_i, X_i) and (y_i, Y_i) are weighted differently. The fading memory factor (γ) allows the algorithm to emphasize on more recent measurements. This will help the algorithm adapt to the true changes in capacity as it degrades over time. The Jacobian of (6) is used to find the roots with the lowest value for $\hat{Q}$ and get the capacity estimate. The Hessian of (6) gives the error bounds of the capacity estimate obtained by the Jacobian. As the AWTLS is an approximation of the WTLS solution based on the weighting of σ_x^2 and σ_y^2, it is crucial to feed the correct variances for both the JEKFCF SoC estimates and the coulomb-counting measurements.

B. Extended Kalman Filter

The degrading capacity of a Li-ion cell shows a non-linear behavior as the charge throughput increases. This is because the cell is cycled and stored under various conditions. This behavior of the degrading capacity as function of Full Equivalent Cycles (FECs) or storage time can be used with an Extended Kalman Filter (EKF) for estimating the degrading capacity. An EKF with the state vector as the degrading capacity (Q) in Ah is formulated as follows:

$$\hat{Q}_k^- = \hat{Q}_{k-1}^+ - \triangle Q + W_k, \tag{7}$$

$$y_k = \hat{Q}_k^- + V_k \tag{8}$$

where, (7) and (8) are the state and output equations respectively. Here, y_k is the direct feed-through of the a priori capacity estimation, W_k is fictitious process noise and V_k is measurement noise. $\triangle Q$ is the difference between the

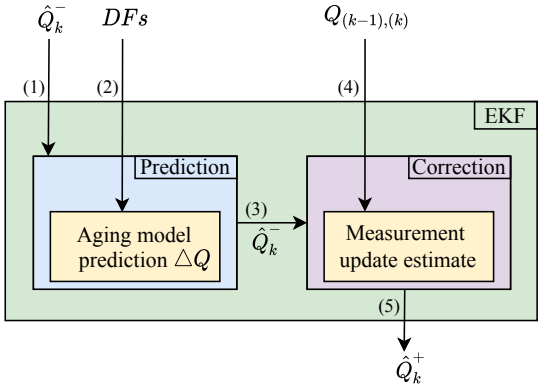

Fig. 7. Extended Kalman Filter formulation for Li-ion capacity estimation with an aging model that uses the Degrading Factors (DFs) as an input.

posteriori estimate of the EKF at time step $k-1$ and the capacity predicted by an aging model $(\widetilde{Q}_k)$ at time step k expressed as:

$$\triangle Q = \frac{\hat{Q}_{k-1}^+ - \widetilde{Q}_k}{\hat{Q}_{k-1}^+} \tag{9}$$

This will be elaborated later in this section. Fig. 7 presents the formulation of this EKF for capacity estimation. Here, a dynamic aging model is used that takes into account calendar and cycle aging Degradation Factors (DFs) presented in Fig. 1. The aging model uses these factors over a time step to assess and predict the cell's health.

The measured capacity $Q_{(k-1),(k)}$ between time steps $k-1$ and k is given by:

$$Q_{(k-1),(k)} = \frac{\int_{k-1}^{k} \frac{\eta i(\tau)}{3600} d\tau}{z\,(k) - z(\,k-1)} \tag{10}$$

Where, $z(k-1)$ and $z(k)$ are the SoC estimates obtained from JEKFCF. The prediction and correction step equations are further derived in a similar way as illustrated in [3]. Therefore, it can be observed that the EKF compares the measured capacity (10) with the capacity predicted by a dynamic aging model (7).

The measurements from the BMS can be used to construct mapping features that can differentiate between calendar and cycle aging. Therefore, it would be appropriate to use a (semi)empirical model to factor the degradation based on calendar and cycle aging. Schmalstieg et al. [10] presented the Holistic aging model that characterizes calendar aging and cycle aging separately. From Fig. 8, it can be seen that calendar aging is defined as a function of storage voltage and temperature and cycle aging is defined as a function of Depth-of-Discharge (DoD), average voltage (ϕV) and the charge throughput of the cell in Ah. The Holistic model presents fitting equations for both capacity degradation and rise in cell impedance. As SoH is defined as per (1), the impedance fitting part of Holistic model is not used.

The Holistic model presents calendar aging (11) and cycle aging (12) fitting equations to characterize the degradation.

$$C_{\text{cal}} = 1 - \alpha_{\text{cap}}(T, V) \cdot t^{\mu} \tag{11}$$

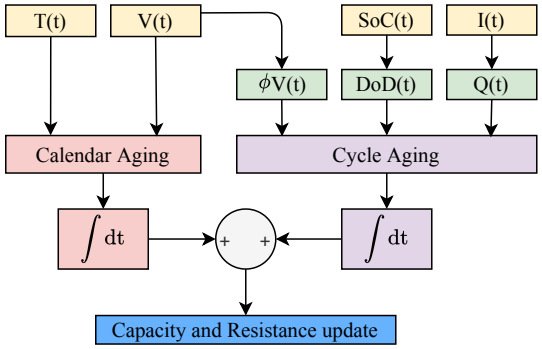

Fig. 8. Measurements and mapping features used by the Holistic aging model.

$$C_{\text{cyc}} = 1 - \beta_{\text{cap}}(\delta D, \phi V) \cdot CT^{\nu} \tag{12}$$

Here α_{cap} is a fitting parameter obtained by fitting storage voltage and temperature. Time t (days) with an exponent value of μ is used to fit the degraded capacity. β_{cap} is a fitting parameter obtained as a function of δD (DoD) and ϕV where ϕV is the average voltage around which the cell is cycled at a particular DoD. The charge throughput of the cell is represented by CT raised to the exponential value of ν is used to fit the equation. As the cell is being cycled at any given DoD and/or ϕV and a particular temperature, time is always passing by. Therefore, during cycling, calendar aging also occurs. Due to this, (11) and (12) need to be superimposed. That gives us the total aging fit function as shown in (13). The parameters and constants of (13) are the DFs used by the Holistic aging model.

$$C_{\text{total}} = 1 - \underbrace{\alpha_{\text{cap}}(T, V) \cdot t^{\mu}}_{Calendar\ aging} - \underbrace{\beta_{\text{cap}}(\delta D, \phi V) \cdot CT^{\nu}}_{Cycle\ aging} \tag{13}$$

The SLIDE program was used to simulate calendar aging and cycle aging under various conditions. A high-energy Li-ion NMC 18650 cell manufactured by Kokam with a nominal capacity of 2.7 Ah was used to simulate the aging behavior. For calendar aging it can be seen from Fig. 9 that the rate of degradation depends on factors like the storage SoC/voltage and the temperature. For cycle aging, from Fig. 10 it can be seen that the rate of capacity degradation depends on factors like DoD, average voltage (ϕV) around which the cell is cycled. For calendar aging, $\alpha_{\text{cap}}(T, V)$ was characterized as a function of T and V. The MATLAB curve fitting tool was used to obtain to fit (11) with μ = 0.58. For cycle aging, it was observed that DoD did not show a linear behavior against β_{cap} as presented in [10]. One of the possible reasons for this can be that the electrochemical models used by SLIDE were not able to capture the true behavior of the cell while generating the data. Therefore, a constant value of $\beta_{\text{cap}}(\delta D, \phi V)$ was used instead of a dynamic function. Similarly, (12) was fitted with ν = 0.85. Therefore, the predicted capacity by the dynamic aging model expressed in (9) can now be obtained as:

$$\widetilde{Q}_{\text{k}} = Q_{\text{nom}} \times C_{\text{total,k}} \tag{14}$$

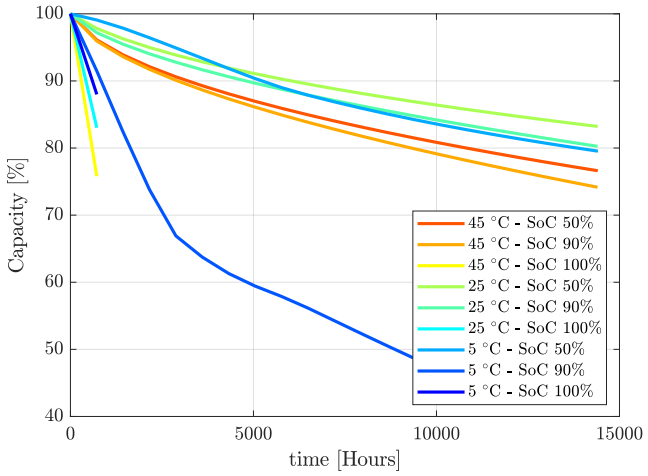

Fig. 9. Calendar aging capacity degradation at various storage T and SoC simulated using SLIDE.

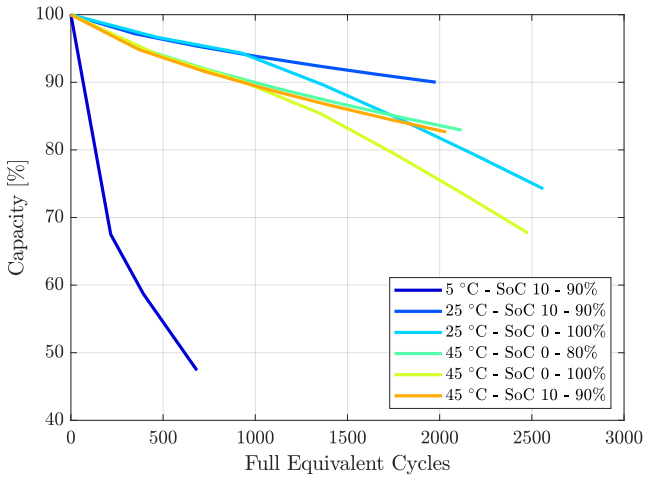

Fig. 10. Cycle aging capacity degradation (at 1C charge and discharge) at various T and DoDs simulated using SLIDE.

Here, Q_{nom} is the nominal capacity of the cell in Ah and $C_{\text{total,k}}$ is the remaining capacity fraction predicted by the holistic aging model (13) at time step k. As the capacity of the Li-ion cell degrades rather slowly over time, this EKF is intended to be triggered based on an event. For example, as the BMS keeps track of the charge throughput via coulomb-counting, the EKF can be triggered after a certain amount of charge throughput has been reached.

C. Sigma-Point Kalman Filters

The EKF performs local analytic linearization at each point in time. While evaluating the estimates of the output of a non-linear function, the EKF assumes that the expected value (mean) of the non-linear function is equal to the value of function at the mean, i.e. $\mathbb{E}[f(x)] \approx f(\mathbb{E}[x])$. This assumption does not hold for all functions and only holds when the function is linear. The accuracy of EKF decreases as the non-linearity of the function increases. This might very well the case when it comes to capacity degradation during most of

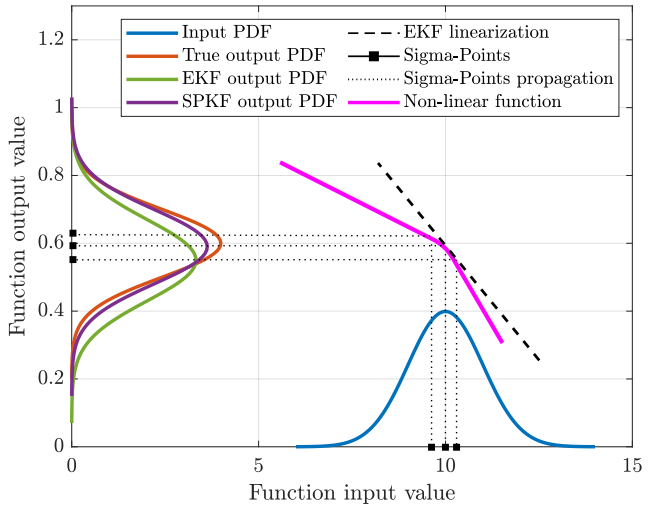

Fig. 11. A comparison of EKF linearization and SPKF propagation for a non-linear function

the lifetime of a li-ion cell. The factors of (13) affect the non-linearity as they are updated dynamically. However, if more constants and fitting parameters are added to (13) in order to obtain a better fit then the non-linearity of characterization rises. The extent of non-linearity of capacity degradation can be therefore quantified with (13). The EKF uses Taylor-series expansion for local linearization as shown in Fig. 11. The higher-order terms of this expansion are not considered. This affects the accuracy of the covariance estimate if the function is highly non-linear. Due to this, once again, the EKF works better when the function is mildly non-linear.

To solve this, Plett [16] presented the Sigma-Point approach to Kalman Filtering (SPKF) for state estimation of a Li-ion cell. This is adopted as an improvement for a better accuracy of the estimates with comparable computational complexity. The Sigma-Point approach does not take into account the assumptions made by the EKF. The SPKF approach does not require to compute the derivatives of the non-linear function. Also, the non-linear function need not be differentiable. A set of input Sigma-Points are carefully chosen from the input Probability Distribution Function (PDF) of the non-linear function for a given time instant. These Sigma-Points are the *weighted* mean and the covariance for that time instant derived from the PDF of the function. These points should be chosen in a particular way that they match the true mean and covariance of the function. These selected points are propagated through the non-linear function. The input Sigma-Points are represented by:

$$\mathcal{S}_{\text{input}} = \{\bar{x},\ \bar{x} + \gamma\sqrt{\Sigma_{\tilde{x}}},\ \bar{x} - \gamma\sqrt{\Sigma_{\tilde{x}}}\} \tag{15}$$

Here, $\bar{x}$ is the mean (vector) of the input PDF. $\sqrt{\Sigma_{\tilde{x}}}$ is the covariance matrix weighted by the factor γ. Here, γ can be one or more parameters depending on the type of SPKF. Practically, $\mathcal{S}_{\text{input}}$ is a set of vectors. The notation $\bar{x} + \gamma\sqrt{\Sigma_{\tilde{x}}}$ means that the vector $\bar{x}$ is added to every column of $\gamma\sqrt{\Sigma_{\tilde{x}}}$. For a system with one state (L), the set $\mathcal{S}_{\text{input}}$ has the mean as the first element. The next L elements are $\bar{x} + \gamma\sqrt{\Sigma_{\tilde{x}}}$ followed by another L elements as $\bar{x} - \gamma\sqrt{\Sigma_{\tilde{x}}}$ resulting in a total of $2L$ + 1 elements. The set of $\mathcal{S}_{\text{input}}$ is presented by black squares on the x-axis in Fig. 11. Where the middle square is the mean and the two squares around the mean represent the covariance. To ensure the weighted mean and covariance is equal to the true mean and covariance we use,

$$\bar{x} = \sum_{\text{i}=0}^{2\text{L}} \alpha_{\text{i}}^{(\text{m})} \mathcal{S}_{\text{i,input}} \tag{16}$$

$$\Sigma_{\tilde{x}} = \sum_{\text{i}=0}^{2\text{L}} \alpha_{\text{i}}^{(\text{c})} \left(\mathcal{S}_{\text{i,input}} - \bar{x}\right)\left(\mathcal{S}_{\text{i,input}} - \bar{x}\right)^{\text{T}} \tag{17}$$

where the factors $\alpha_{\text{i}}^{(\text{m})}$ and $\alpha_{\text{i}}^{(\text{c})}$ are weighting constants used when computing the mean and the covariance respectively. Therefore, γ, $\alpha_{\text{i}}^{(\text{m})}$ and $\alpha_{\text{i}}^{(\text{c})}$ are the tuning parameters for the SPKF. The output Sigma-Points can be calculated by evaluating the function at every input Sigma-Point i.e.

$$\mathcal{S}_{\text{i,output}} = f(\mathcal{S}_{\text{i,input}}) \tag{18}$$

This process is called as Unscented Transformation (UT) where the set of $\mathcal{S}_{\text{input}}$ is propagated through a non-linear function. The UT is illustrated in Fig. 11 by the dotted lines that propagate the $\mathcal{S}_{\text{input}}$ points through the non-linear function to obtain the $\mathcal{S}_{\text{output}}$ points that form the output PDF. Similarly, the output mean and the covariance can be computed by using

$$\bar{y} = \sum_{\text{i}=0}^{2\text{L}} \alpha_{\text{i}}^{(\text{m})} \mathcal{S}_{\text{i,output}} \tag{19}$$

$$\Sigma_{\tilde{y}} = \sum_{\text{i}=0}^{2\text{L}} \alpha_{\text{i}}^{(\text{c})} \left(\mathcal{S}_{\text{i,output}} - \bar{y}\right)\left(\mathcal{S}_{\text{i,output}} - \bar{y}\right)^{\text{T}} \tag{20}$$

where $\bar{y}$ is the mean and $\Sigma_{\tilde{y}}$ is the covariance of the output PDF respectively. The Central-Difference Kalman Filter (CDKF) and the Unscented Kalman Filter (UKF) are two such variants of the Sigma-Point Kalman Filter approach. The CDKF and UKF differ in the way these Sigma-Points are selected with the weighting factor γ.

1) CDKF: Table I illustrates the SPKF tuning parmeters. The CDKF has only one tuning parameter h. In practice, the value of h can take any positive value but it is set to $\sqrt{3}$ for a Gaussian distribution. Here, the covariance is weighted by a factor of h. This weighting illustrates the spread of covariance around the mean as the *centre*, therefore the name Central-Difference Kalman Filter. This is the reason,

TABLE I
SPKF TUNING PARAMETERS.

	γ	$\alpha_0^{(\text{m})}$	$\alpha_{\text{k}}^{(\text{m})}$	$\alpha_0^{(\text{c})}$	$\alpha_{\text{k}}^{(\text{c})}$
CDKF	h	$\frac{h^2-L}{h^2}$	$\frac{1}{2h^2}$	$\frac{h^2-L}{h^2}$	$\frac{1}{2h^2}$
UKF	$\sqrt{L+\lambda}$	$\frac{\lambda}{\gamma^2}$	$\frac{1}{2\gamma^2}$	$\frac{\lambda}{\gamma^2} + \left(1-\alpha^2+\beta\right)$	$\frac{1}{2\gamma^2}$

TABLE II
DESCRIPTION OF UKF TUNING PARAMETERS.

Parameter	Role	Range/Value
α	Primary scaling parameter	$10^{-2} \leq \alpha \leq 1$
κ	Secondary tuning parameter	1
β	Prior information of the PDF	2 (for Gaussian PDF)

the CDKF performs well for Gaussian distributions. A CDKF is constructed in the same way as expressed in (7) and (8) and used in an event-based manner with the holistic aging model.

2) UKF: The UKF provides a higher number of tuning parameters to choose these Sigma-Points as opposed to CDKF. The parameters λ, α and κ influence the spread of Sigma-Points around the mean. The parameter λ is expressed in terms of α, κ and the number of states L as

$$\lambda = \alpha^2(L + \kappa) - L \tag{21}$$

For Gaussian distributions, β is set to 2. Table II describes the range/values of the these parameters.

It needs to be noted that the tuning parameter α is different from $\alpha_0^{(m)}$, $\alpha_k^{(m)}$, $\alpha_0^{(c)}$ and $\alpha_k^{(c)}$. An UKF is constructed in the same way as the CDKF with state and output equations illustrated in (7) and (8) respectively. It can be observed that the UKF has more parameters to express the distribution with the near same computational complexity as that of CDKF.

V. COMPARISON OF SOH ALGORITHMS

Acquiring Li-ion cell aging measurement data is a time intensive and error prone process. Programmable cell testers and climate (temperature) chambers are required to test Li-ion cells under certain (dis)charge and temperature conditions respectively. Therefore, using a computer simulation program like SLIDE not only saves time but also allows to generate aging data in a precisely controlled way. The SLIDE simulator was used to cycle the cell till the capacity is lost to 80% of its nominal capacity. Measurements are recorded at 1 Hz. The Urban Dynamometer Driving Schedule (UDDS) drive cycle was chosen as it comprises of a few 2-3C discharge pulses and regenerative charge pulses that are greater than 1C. However, it needs to be noted that a (dis)charge current of greater than 3C is not supported well by SLIDE and may possibly result in erroneous data generation.

Table III presents the test configuration. The SLIDE simulator was programmed to repeatedly cycle the cell with the UDDS profile till 2.75 V. Capacity checks were programmed to be conducted every 5 FECs to create a finer reference for comparing the capacity estimation. All the tests described in table III were performed at 25°C.

TABLE III
TESTING REGIME.

	Profile	Start	End
Discharge	UDDS	4.25 V	2.75 V
Charge	1C CCCV	2.75 V	0.05C cut-off
Check-up	0.04C CCCV	4.25 V	0.005C cut-off

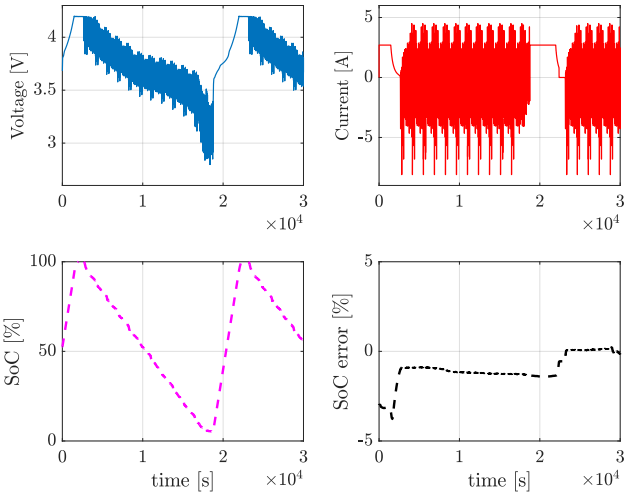

Fig. 12. Voltage and current data generated from SLIDE with JEKFCF SoC estimation

Fig. 12 presents the voltage and current data generated from SLIDE at 1 Hz. The voltage and current data is used as an input for the JEKFCF SoC estimation. Fig. 13 presents the estimation and feedback flow of the JEKFCF SoC estimation and capacity estimation with all the aforementioned algorithms. Note that the AWTLS algorithm does not use the Holistic aging model. However, all the three KF variants use the Holistic aging model given their formulation. Therefore, in order to implement any of the three KF variants, the user has to first characterize the cell for the aging model to obtain the fitting parameters for (13).

For AWTLS, a SoC estimation window of 80% to 20% is selected during every discharge cycle. For a fixed value of (dis)charged coulombs (y_i), its equivalent $\triangle$SoC (x_i) was fed as an input to the AWTLS algorithm repeatedly starting from SoC 80% till SoC 20%. The AWTLS was only able to capture the degrading trend in capacity when data from only the discharge cycle was used as an input. Therefore, N values of (x_i, y_i) pairs were obtained between the previous time step $k-1$ (SoC = 80%) and the current time step k (SoC = 20%)

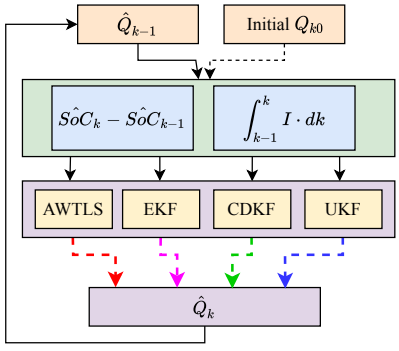

Fig. 13. Capacity estimation and feedback flowchart

for every discharge cycle. The AWTLS also requires the variance of both SoC estimates and that of coulomb counting measurements. A SoC variance of $\sigma_x = 0.03$ (3%) is selected as several experiments with SLIDE data and the JEKFCF revealed a maximum SoC estimation error of $\pm$ 3%. For a coulomb counting, a variance of $\sigma_x = 0.001$ was used as the data was generated from a simulation and there was no current sensor bias to be corrected. The capacity estimate obtained from these algorithms is used as an input for the SoC estimation in the next time step. Therefore, the JEFKCF SoC estimation was fed with an updated capacity estimate every cycle. This is rather important and accurate as the SoC needs to be estimated for the degraded capacity and not the nominal capacity. Fig. 14 presents the AWTLS estimation with the goodness of fit evaluation for 200 FECs. Transient peaks can be observed for the capacity estimation from the AWTLS algorithm. The goodness of fit is calculated by evaluating the incomplete gamma function in order to check how good the hypothesized model fits the measured data with the variances. The goodness of model fit can be dynamically evaluated to get an approximate feedback of the quality of capacity estimations. If the goodness of fit is < 0.95, there is a high probability that the capacity estimations will not be accurate due to a rather high error in either the coulomb counting measurements or the SoC estimations.

From Fig. 15, it is observed that the reason for the peaks was a comparatively higher SoC estimation error. This can be a result of bad model fit of the JEKFCF for the measured voltage and current. The SoC estimation error can be reduced by tuning the JEKFCF forgetting factor, however this cannot be done dynamically during run-time. Moreover, the SoC estimation error was greater than the SoC variance that was used as an input to the AWTLS algorithm. Due to this, the AWTLS algorithm is not able to fit the input data accurately. As the peaks are not mitigated by feeding a higher SoC variance, it can be concluded that a rather accurate SoC estimation is required as an input for the AWTLS algorithm.

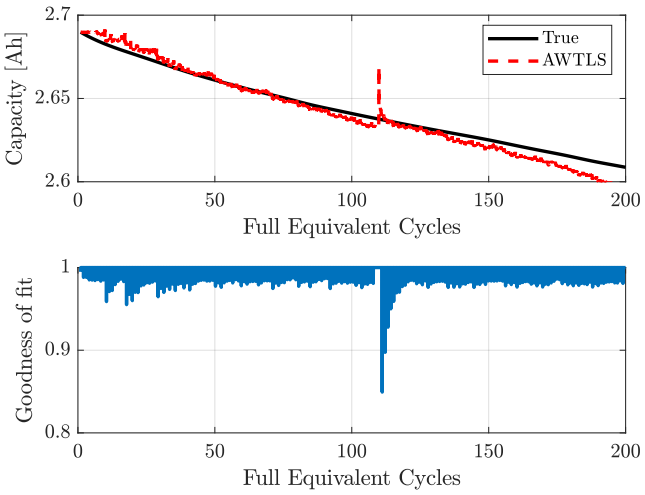

Fig. 14. AWTLS estimation for 200 FECs with Goodness of Fit

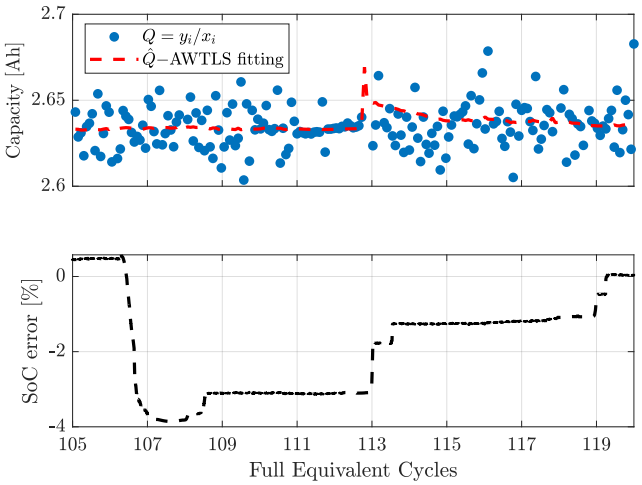

Fig. 15. Transient peaks in AWTLS capacity fitting with SoC estimation error

This can then be remedied by skipping the capacity estimation update for the time step when the goodness of model fit is < 0.95.

The AWTLS algorithm is equipped with a forgetting factor $(0<\gamma\leq 1)$. This can be used to tune the algorithm to emphasize on more recent measurements. Secondly, the (dis)charged coulombs (y_i) can be varied to observe its effect on estimation accuracy. Fig. 16 presents the AWTLS capacity estimation root-mean-square error for 200 FECs with various forgetting factors and various fixed (dis)charged coulombs. It can be observed that a forgetting factor of $\gamma = 0.975$ with $y_i = 250$ A.s is the most accurate for this experiment. For cell with 2.7 Ah nominal capacity, it can be safely noted that a coulomb-counting measurement of 250 A.s is large enough to get an equivalent $\triangle$SoC for capturing a degrading trend in the measurements and the SoC estimations respectively. Increasing the couloumb-counting range further results in a higher RMSE. No concrete conclusion can be drawn for this behavior given

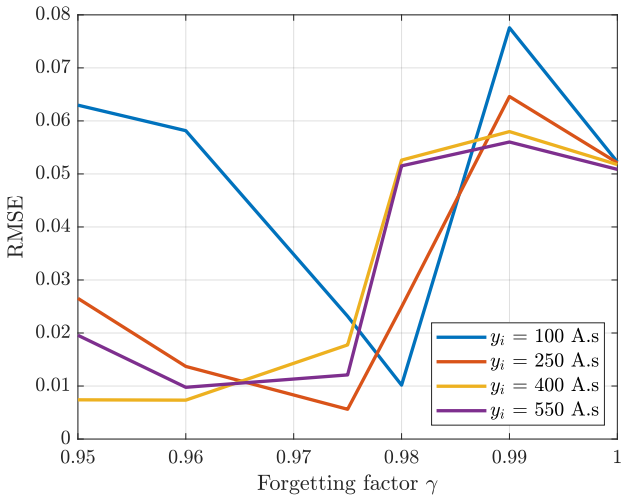

Fig. 16. A comparison of the AWTLS algorithm using various forgetting factors and coulomb-counting measurements as input for 200 FECs

the data presented in Fig. 16

For the KF variants, capacity estimation was conducted during every discharge cycle with a window of 80% $(k-1)$ to 20% (k) and also during every charge cycle with a window of 20% $(k-1)$ to 80% (k). The three KF variants were initialized with a wrong capacity. Fig. 17 presents KF variants' capacity estimation for 200 FECs. It can be observed that all the three variants show a rather similar behavior. They quickly converge to the near-correct capacity estimate within 10 iterations. The $3\sqrt{\sum Q}$ bounds provide a 99.7% confidence interval for the capacity estimation. It can be observed that the KF variants can avoid a large sudden spike (at cycle 113) in the capacity estimation as compared to the AWTLS algorithm. The UKF is the least susceptible to an erroneous SoC estimation. Morever, UKF estimates more tighter $3\sqrt{\sum Q}$ bounds as compared to EKF and CDKF. Therefore, only the $3\sqrt{\sum Q}$ bounds of UKF are show in Fig. 17. This is because these erroneous SoC estimations result in either a transient non-Gaussian distribution or a combination of two Gaussian distributions. The UKF having a higher number of tuning parameters can propagate the mean and the covariance with the Sigma-Points to the output PDF rather accurately as compared to the EKF and the CDKF.

Fig. 18 presents the comparison of the capacity estimation of the four algorithms for 1000 FECs. For a fair comparison, all the four algorithms were tested on the same data-set generated by SLIDE for 1000 FECs with the testing regime shown in table III at 25°C. For AWTLS, as before, it can be observed that the capacity estimation is highly susceptible to SoC estimation errors (between cycles 800 to 1000). A SoC estimation error of $> 3\%$ results in an significantly wrong capacity estimation. The three KF variants are more robust as compared to the AWTLS as the aging model factors in the degradation based on the characterization. The peaks in AWTLS capacity estimation result in an error of $> 1\%$. Therefore, this erroneous capacity estimation is not recommended to be used as an input for SoF estimation. The peaks also result in

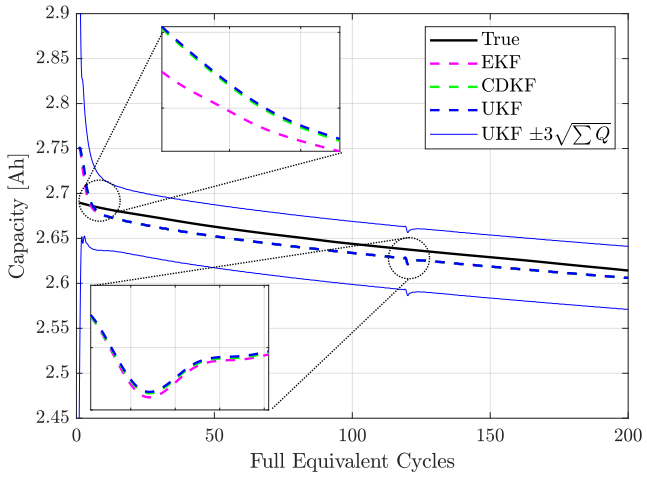

Fig. 17. Capacity estimation with EKF, CDKF and UKF with $3\sqrt{\sum Q}$ bounds for 200 FECs

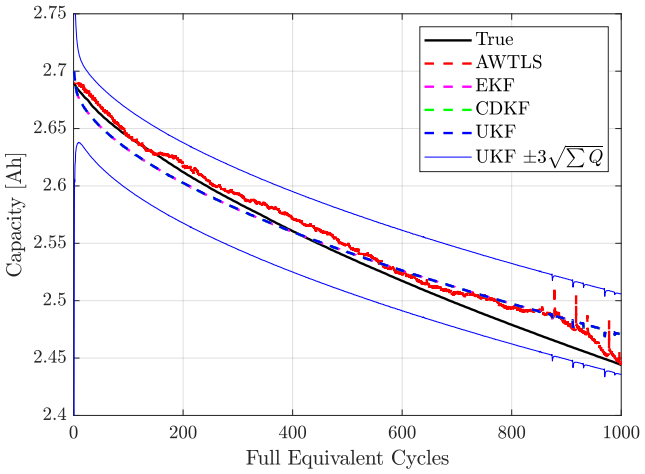

Fig. 18. Capacity estimation comparison of the implemented algorithms for 1000 FECs.

TABLE IV
ROOT-MEAN-SQUARE ERROR COMPARISON FOR 1000 CYCLES

AWTLS	EKF	CDKF	UKF
0.0110	0.0139	0.0139	0.0139

a bad model fit of < 0.95 as shown in Fig. 15. For the three KF variants, the transient error caused due to an erroneous SoC estimation is $< 0.5\%$. It can be also observed that the KF variants recover from this error and converge to the near-accurate capacity estimate. Therefore, they are more robust to an erroneous SoC estimate as compared to the AWTLS capacity estimation.

Table IV presents the root-mean-square error (RMSE) comparison of AWTLS and the three KF variants. The AWTLS performs the best in terms of RMSE. Although, some transient peaks can give a higher RMSE than the three KF variants. The EKF, CDKF and UKF perform nearly the same as the distribution caused by the cell behaviour of the capacity is highly Gaussian except for a few times when the SoC estimation error is large.

VI. Implementation Complexity

Besides comparing the accuracy of the selected SoH estimation algorithms, an observation can also be made regarding the implementation complexity of these algorithms. This is important as these algorithms are conceived as software tasks that are intended to be implemented on a resource-constrained embedded micro-controller that is a part of the BMS. Such tasks are typically realised using a round-robin scheduler or a (non)preemptive scheduler to satisfy real-time firmware requirements. For such an embedded implementation, resources like processor attention and memory are at a premium. Therefore, it is important to compare these algorithms based on their embedded implementation. Table V presents the quantitative implementation complexity of the SoH algorithms. As mentioned earlier, the AWTLS algorithm does not require any prior characterization of Li-ion cell aging data. The three

TABLE V
IMPLEMENTATION COMPLEXITY OF SOH ALGORITHMS.

	AWTLS	EKF	CDKF	UKF
Characterization (offline)	Low	High	High	High
Implementation (online)	Medium	Low	Medium	Medium

KF variants on the other hand require the characterization of the holistic aging model. Therefore, the offline characterization complexity is high.

The majority of these micro-controllers run on C code whereas the algorithms are primarily tested with MATLAB. The MATLAB code needs to be translated to C code. Moreover, this C code needs to be optimized for a target micro-controller. An example of such an optimization is the Fixed-point analysis of all the variables used by the code and using the correct compiler settings. The AWTLS requires to solve a quartic equation along with evaluating an incomplete gamma function. These are processor-intensive tasks for some low-power micro-controller variants. The EKF on the other hand largely uses matrix arithmetic operations. The SPKF variants require to compute a Cholesky decomposition of the covariance matrix. Because of this, the C code complexity is medium for AWTLS, CDKF and UKF. The EKF has the lowest C code complexity of all.

VII. CONCLUSIONS AND FUTURE WORK

In this study, several algorithms for the capacity estimation were implemented, tested and compared. The AWTLS provides a recursive approach that factors the uncertainties in both coulomb counting measurement and SoC estimations. It does not require any prior characterization of the cell. A robust SoC estimation algorithm needs to be used when using SoC estimations as an input for the AWTLS algorithm. However, the AWTLS capacity estimation is not stable if the SoC estimation inputs are not accurate. The three KF variants make use of the Holistic aging model. This provides a more robust capacity estimation. It needs to be noted that characterizing the holistic aging model needs the cell's lifetime data. This is a rather time-intensive process. Therefore, accelerated aging tests need to be conducted to obtain such data. This was remedied in this study by using the SLIDE simulator program. To conclude, the AWTLS algorithm can be used as a quick solution for capacity estimations if the SoC estimations are accurate. On the other hand, if the SoC estimations are not accurate or if they cannot be trusted, the UKF will result in a lower RMSE as compared to the AWTLS algorithm. This comes at the cost of characterizing aging data of the Li-ion cell.

The SoH was based wholly and solely on the cell capacity estimations. In the future, the SoH can be defined based on both capacity and impedance estimations. For impedance, the JEKFCF SoC estimation can be used to estimate the cell impedance as it is one of the jointly estimated model parameters with the SoC. The Holistic aging model also provides similar fitting equations for cell impedance. Therefore, a combination of cell capacity and impedance estimates can provide an even better and robust estimation of the SoH. The tests conducted in this study were at 25°C. As temperature affects the rate of degradation, more tests need to be conducted at various temperatures. Finally, validation of these algorithms on real cell measurement data would be required to further solidify the conclusions.

REFERENCES

[1] U. Krewer, F. Röder, E. Harinath, R. D. Braatz, B. Bedürftig, and R. Findeisen, "Review—dynamic models of li-ion batteries for diagnosis and operation: A review and perspective," *Journal of The Electrochemical Society*, vol. 165, no. 16, 2018.

[2] A. Farmann, W. Waag, A. Marongiu, and D. U. Sauer, "Critical review of on-board capacity estimation techniques for lithium-ion batteries in electric and hybrid electric vehicles," *Journal of Power Sources*, vol. 281, May 2015.

[3] G. L. Plett, "Extended kalman filtering for battery management systems of LiPB-based HEV battery packs," *Journal of Power Sources*, vol. 134, no. 2, Aug. 2004.

[4] L. Fang, J. Li, and B. Peng, "Online estimation and error analysis of both SOC and SOH of lithium-ion battery based on DEKF method," *Energy Procedia*, vol. 158, Feb. 2019.

[5] G. L. Plett, "Recursive approximate weighted total least squares estimation of battery cell total capacity," *Journal of Power Sources*, vol. 196, no. 4, Feb. 2011.

[6] D. Liu, X. Yin, Y. Song, W. Liu, and Y. Peng, "An on-line state of health estimation of lithium-ion battery using unscented particle filter," *IEEE Access*, vol. 6, 2018.

[7] N. Harting, R. Schenkendorf, N. Wolff, and U. Krewer, "State-of-health identification of lithium-ion batteries based on nonlinear frequency response analysis: First steps with machine learning," *Applied Sciences*, vol. 8, no. 5, May 2018.

[8] M. Berecibar, M. Garmendia, I. Gandiaga, J. Crego, and I. Villarreal, "State of health estimation algorithm of LiFePO4 battery packs based on differential voltage curves for battery management system application," *Energy*, vol. 103, May 2016.

[9] C. R. Birkl, M. R. Roberts, E. McTurk, P. G. Bruce, and D. A. Howey, "Degradation diagnostics for lithium ion cells," *Journal of Power Sources*, vol. 341, Feb. 2017.

[10] J. Schmalstieg, S. Käbitz, M. Ecker, and D. U. Sauer, "A holistic aging model for li(NiMnCo)o2 based 18650 lithium-ion batteries," *Journal of Power Sources*, vol. 257, Jul. 2014.

[11] "Wide range fuel gauge with impedance track™ technology," Texas Instruments, 12 2012, rev. B.

[12] K. Dadhekar, "Synchronous voltage and current measurement of li-ion battery packs for enhanced state of charge estimation," Eindhoven University of Technology, MSc. internship report, 2019.

[13] J. M. Reniers, G. Mulder, and D. A. Howey, "Review and performance comparison of mechanical-chemical degradation models for lithium-ion batteries," *Journal of The Electrochemical Society*, vol. 166, no. 14, 2019.

[14] S. Qu, Y. Kang, P. Gu, C. Zhang, and B. Duan, "A fast online state of health estimation method for lithium-ion batteries based on incremental capacity analysis," *Energies*, vol. 12, no. 17, Aug. 2019.

[15] H. Beelen, "Model-based temperature and state-of-charge estimation for li-ion batteries," Ph.D. dissertation, Department of Electrical Engineering, 9 2019.

[16] G. L. Plett, "Sigma-point kalman filtering for battery management systems of LiPB-based HEV battery packs," *Journal of Power Sources*, vol. 161, no. 2, Oct. 2006.

[17] M. Arulampalam, S. Maskell, N. Gordon, and T. Clapp, "A tutorial on particle filters for online nonlinear/non-gaussian bayesian tracking," *IEEE Transactions on Signal Processing*, vol. 50, no. 2, 2002.

[18] H. Li, D. Pan, and C. L. P. Chen, "Intelligent prognostics for battery health monitoring using the mean entropy and relevance vector machine," *IEEE Transactions on Systems, Man, and Cybernetics: Systems*, vol. 44, no. 7, Jul. 2014.

[19] Y. Choi, S. Ryu, K. Park, and H. Kim, "Machine learning-based lithium-ion battery capacity estimation exploiting multi-channel charging profiles," *IEEE Access*, vol. 7, 2019.